Oxo-Bridged Linear Diosmium Complexes with Unsymmetric Ligand Environment. Structures of the Diosmium(IV,IV) Complex $[(py)_2Cl_2(CH_3COO)Os(\mu\text{-}O)Os(py)_2Cl_3]$ (py = Pyridine) and Its Mixed-Valence (III,IV) Analog

Yoichi Imbe, Keisuke Umakoshi,* Chikako Matsunami, and Yoichi Sasaki*

Department of Chemistry, Faculty of Science, Hokkaido University, Kita-ku, Sapporo 060, Japan

Received July 28, 1994[⊗]

A new (μ-oxo)diosmium(IV) complex with unsymmetric ligand environment, $[Os^{IV}_2(\mu\text{-}O)Cl_5(CH_3CO_2)(py)_4]$ (**2**), and its one electron reduced species $(Et_4N)[Os^{III}Os^{IV}(\mu\text{-}O)Cl_5(CH_3CO_2)(py)_4]$ ((Et_4N)[**3**]) have been prepared and characterized by several physical methods. X-ray crystallography was conducted for **2** and (Et_4N)[**3**] as well as the osmium(VI) complex $[OsO_2Cl_2(py)_2]$ (**1**). **1** takes a trans-dioxo structure with both the pyridine and chloro ligands in a *cis* configuration. The reaction of **1** with refluxing $CH_3COOH/(CH_3CO)_2O$ mixtures provided **2** with the linear Os−O−Os moiety in which trans positions to the oxide bridge are occupied by monodentate acetate for one osmium ion and chloride for another. Cyclic voltammetry showed that **2** is oxidized irreversibly at E_{pa} = +1.68 V, and is reduced reversibly and quasi-reversibly at $E_{1/2}{}^1$ = +0.03 and $E_{1/2}{}^2$ = −1.15 V vs Ag/AgCl, respectively, in acetonitrile. The compound **2** is reduced chemically as well as electrochemically to the mixed-valence compound, $[\mathbf{3}]^-$. The complex anion $[\mathbf{3}]^-$ crystallizes with Et_4N^+ in a 1:1 ratio. The average oxidation state of osmium ions is +3.5. The structure of $[\mathbf{3}]^-$ is very similar to that of **2** except that all bond lengths parallel to the Os−O−Os axis are elongated. Differences in the two Os−O distances are much more evident in **2** rather than $[\mathbf{3}]^-$. Equatorial Os−N and Os−Cl distances of the two osmium pseudooctahedra in **2** are respectively virtually identical and are only slightly changed on reduction to $[\mathbf{3}]^-$. No splitting of the peak was observed in the X-ray photoelectron spectrum of $[\mathbf{3}]^-$ in the Os($4f_{7/2}$) region. The odd electron in $[\mathbf{3}]^-$ is delocalized on the two osmium atoms. Crystal data: $[OsO_2Cl_2(py)_2]$, tetragonal, space group $P4_12_12$, a = 10.452(1) Å, c = 12.149(1) Å, Z = 4; $[Os^{IV}_2(\mu\text{-}O)Cl_5(CH_3CO_2)(py)_4]$, monoclinic, space group $P2_1/c$, a = 18.007(2) Å, b = 10.378(2) Å, c = 15.529(2) Å, β = 104.53(1)°, Z = 4; $(Et_4N)[Os^{III}Os^{IV}(\mu\text{-}O)Cl_5(CH_3CO_2)(py)_4]$, orthorhombic, space group *Pcab*, a = 20.895(4) Å, b = 25.120(5) Å, c = 14.149(9) Å, Z = 8.

Introduction

Higher oxidation states of ruthenium and osmium are featured by the coordination of oxide or nitride ion. As a consequence of $d\pi-p\pi$ overlap that produces M−O or M−N multiple bonding, metal ions in higher oxidation state are stabilized.[1] Oxide or nitride ions also serve as bridging ligands to produce μ-oxo or μ-nitrido dinuclear complexes, respectively, with linear or bent M−O−M or M−N−M cores (M = Ru, Os).

In the case of ruthenium, oxo-bridged dimers often take doubly or triply bridged structures by the cooperation of additional oxide or other bridging ligands.[2-5] Among such multi-bridged compounds, (μ-oxo)bis(μ-carboxylato)diruthenium complexes are particularly interesting because of their structural relevance to some metalloenzymes such as hemerythrin and also their versatile spectroscopic and redox properties.[6-17] The only known diosmium complexes of this type are osmium(IV) dimers, $[Os_2(\mu\text{-}O)(\mu\text{-}RCOO)_2X_4(PR'_3)_2]$ ($R = CH_3, C_2H_5$; X = Cl, Br; $PR'_3 = PPh_3, PEt_2Ph$).[18] These diosmium(IV) complexes were prepared by refluxing an osmium(VI) complex, $[OsO_2X_2(PR'_3)_2]$, in a $RCOOH-(RCOO)_2O$ mixture. Since this is the only preparation method known to access to the (μ-oxo)bis(μ-carboxylato)diosmium core, it would be worth investigating if other dioxo−Os(VI) complexes also provide this diosmium structural core.

We have found, however, that the reaction of $[OsO_2Cl_2(py)_2]$ (py = pyridine)[19] with a $CH_3COOH-(CH_3CO)_2O$ mixture results in the formation of linear μ-oxo diosmium(IV) complexes with the coordination of acetate trans to the oxide bridge instead of the cis position necessary for the bridge formation. Nevertheless, the new complexes provide various interesting informa-

[⊗] Abstract published in *Advance ACS Abstracts,* January 15, 1995.

(1) Che, C.-M.; Yam, V. W.-W. *Adv. Inorg. Chem.* **1992**, *39*, 233−325.
(2) Fomina, T. A.; Zhilyaev, A. N.; Kuz'menko, I. V.; Chalisova, N. N.; Sobolev, A. N.; Porai-Koshits, M. A.; Baranovskii, I. B. *Russ. J. Inorg. Chem.* **1989**, *34*, 879−882.
(3) Neubold, P.; Della Vedova, B. S. P. C.; Wieghardt, K.; Nuber, B.; Weiss, J. *Inorg. Chem.* **1990**, *29*, 3355−3363.
(4) Kelson, E. P.; Henling, L. M.; Schaefer, W. P.; Labinger, J. A.; Bercaw, J. E. *Inorg. Chem.* **1993**, *32*, 2863−2873.
(5) Geilenkirchen, A.; Neubold, P.; Schneider, R.; Wieghardt, K.; Florke, U.; Haupt, H.-J.; Nuber, B. *J. Chem. Soc., Dalton Trans.* **1994**, 457−464.
(6) Sasaki, Y.; Suzuki, M.; Tokiwa, A.; Ebihara, M.; Yamaguchi, T.; Kabuto, C.; Ito, T. *J. Am. Chem. Soc.* **1988**, *110*, 6251−6252.
(7) Neubold, P.; Wieghardt, K.; Nuber, B.; Weiss, J. *Angew. Chem., Int. Ed. Engl.* **1988**, *27*, 933−935.
(8) Neubold, P.; Wieghardt, K.; Nuber, B.; Weiss, J. *Inorg. Chem.* **1989**, *28*, 459−467.
(9) Llobet, A.; Curry, M. E.; Evans, H. T.; Meyer, T, J, *Inorg. Chem.* **1989**, *28*, 3131−3137.
(10) Das, B. K.; Chakravarty, A. R. *Inorg. Chem.* **1990**, *29*, 2078−2083.
(11) Barral, M. C.; Jimenez-Aparicio, R.; Royer, E. C.; Urbanos, F. A. *Polyhedron* **1991**, *10*, 113−120.
(12) Sasaki, Y.; Suzuki, M.; Nagasawa, A.; Tokiwa, A.; Ebihara, M.; Yamaguchi, T.; Kabuto, C.; Ochi, T.; Ito, T. *Inorg. Chem.* **1991**, *30*, 4903−4908.
(13) Ochi, T.; Sasaki, Y.; Yamaguchi, T.; Ito, T. *Chem. Lett.* **1991**, 2019−2022.
(14) Gupta, N.; Mukerjee, S.; Mahapatra, S.; Ray, M.; Mukherjee, R. *Inorg. Chem.* **1992**, *31*, 139−141.
(15) Syamala, A.; Chakravarty, A. R. *Inorg. Chem.* **1991**, *30*, 4699−4704.
(16) Syamala, A.; Das, B. K.; Chakravarty, A. R. *Polyhedron* **1992**, *11*, 335−339.
(17) Syamala, A.; Chakravarty, A. R. *Polyhedron* **1993**, *12*, 273−278.
(18) Armstrong, J. E.; Robinson, W. R.; Walton, R. A. *Inorg. Chem.* **1983**, *22*, 1301−1306.
(19) El-Hendawy, A. M.; Griffith, W. P.; Taha, F. I.; Moussa, M. N. *J. Chem. Soc., Dalton Trans.* **1989**, 901−906.

0020-1669/95/1334-0813$09.00/0

tion on linear (μ-oxo)diosmium complexes. One of the new complexes serves as the first example of (μ-oxo)diosmium(IV) complex with two osmium ions in different coordination environments. We were also successful in obtaining the first (μ-oxo)diosmium(III,IV) mixed valence complex. X-ray crystal analyses of both the complexes provide a unique structural comparison. This paper reports the preparation, structures, and other properties of these new dinuclear osmium complexes.

Experimental Section

Materials. Osmium tetraoxide (OsO_4) and silica gel (Wakogel C-200) for column chromatography were purchased from Wako Pure Chemical Industries, Ltd. Acetonitrile was dried over calcium hydride and distilled under an argon atmosphere. Tetrabutylammonium perchlorate (TBAP) was recrystallized twice from ethanol. All other commercially available reagents were used as purchased.

$[OsO_2Cl_2(py)_2]$ (1). The procedure of Salmon and Walton for *trans*-$[OsO_2Cl_2(PPh_3)_2]$[20] was adopted for preparing **1** with the use of pyridine in place of triphenylphosphine. Osmium tetraoxide (1.0 g) was dissolved in a mixture of ethanol (30 mL) and concentrated hydrochloric acid (5 mL). To the solution was added 5 mL of pyridine and the reaction mixture was stirred for 5 min at 90 °C. The resulting brownish yellow precipitate was filtered, washed with methanol, water, and diethyl ether, and then dried in vacuo; yield 1.42 g (80%). Recrystallization from DMF/ether gave brownish yellow crystals which were suitable for X-ray structural analysis. IR (KBr)/cm^{-1}: 1610 s, 1490 m, 1454 s, 1408 w, 1362 m, 1354 m, 1246 m, 1216 s, 1158 w, 1104 w, 1072 s, 1024 s, ν(Os=O) 858 s, 770 s, 694 s, 652 m, 454 w, ν(Os−Cl) 328 s, 298 m. UV−vis (DMF)/nm: 269 (ϵ 11 200 M^{-1} cm^{-1}), 314 (1450), 367 sh (506), 463 sh (112). ^{1}H NMR ($(CD_3)_2SO$)/ppm: δ 7.82 (t, 4H), 8.26 (t, 2H), 8.74 (d, 4H). Anal. Calcd for $C_{10}H_{10}Cl_2N_2O_2Os$: C, 26.61; H, 2.23; N, 6.21. Found: C, 26.75; H, 2.19; N, 6.31.

$[Os^{IV}_2(\mu\text{-}O)Cl_5(CH_3CO_2)(py)_4]$ (2). A suspension of **1** (400 mg) in a mixture of acetic acid (27 mL) and acetic anhydride (3 mL) was refluxed for 50 h. The brown solid was collected by evaporating the mixture. This was dissolved in a minimum volume of chloroform. The solution was loaded onto a silica gel column (25 × 3 cm) and eluted with chloroform to give several fractions, four of which gave sufficient amount of eluents. Slow concentration of the third main fraction among the four gave dark greenish yellow crystals of X-ray quality; yield 42 mg (10%). IR (KBr)/cm^{-1}: ν(CO) 1688 s, 1614 s, 1490 m, 1456 s, 1358 m, 1220 s, 1164 m, 1072 m, 1054 w, 1006 m, 976 w, 918 m, 760 m, 688 s, 648 m, 634 m, 602 w, 526 m, 500 m, 482 m, ν(Os−Cl) 330 s. UV−vis (CH_3CN)/nm: 261 (ϵ 16 300 M^{-1}cm^{-1}), 306 (14 700), 335 (14 500), 418 (29 000), 598 (430), 704 (430), 735 (350). ^{1}H NMR (CD_3CN)/ppm: δ 1.65 (s, 3H), 7.33 (t, 8H), 7.67 (tt, 2H), 7.72 (tt, 2H), 8.72 (dd, 4H), 8.76 (dd, 4H). Anal. Calcd for $C_{22}H_{23}Cl_5N_4O_3Os_2$: C, 27.84; H, 2.44; N, 5.90. Found: C, 27.80; H, 2.45; N, 5.90.

$(Et_4N)[Os^{III}Os^{IV}(\mu\text{-}O)Cl_5(CH_3CO_2)(py)_4]$ ((Et_4N)[3]). To a solution of **2** (30 mg) in acetonitrile (10 mL) was added hydrazine monohydrate (2 μL) at 20 °C under an argon atmosphere. The greenish yellow solution turned to orange immediately. Tetraethylammonium bromide (7 mg) was added to the resulting solution. Deep orange crystals of X-ray quality were obtained by a vapor diffusion of diethyl ether. IR (KBr)/cm^{-1}: ν(CO) 1633 s, 1608 m, 1487 m, 1449 s, 1396 w, 1369 s, 1312 s, 1218 w, 1183 w, 1173 w, 1161 w, 1152 m, 1076 w, 1070 w, 1053 w, 1019 m, 1004 w, 846 m, 788 w, 764 s, 690 s, 659 m, 652 m, 534 w, 467 w, 415 w, 374 w, ν(Os−Cl) 310 s. UV−vis (CH_3CN)/nm: 278 (ϵ 20 600 M^{-1} cm^{-1}), 331 sh (13 000), 380 (12 000), 454 (19 200), 685 (720), 819 (650). Anal. Calcd for $C_{30}H_{43}Cl_5N_5O_3Os_2$: C, 33.38; H, 4.02; N, 6.49. Found: C, 33.22; H, 4.00; N, 6.58.

$[Os^{IV}_2(\mu\text{-}O)Cl_4(CH_3CO_2)_2(py)_4]$ (4). As mentioned in the preparation of **2**, four fractions were obtained by the column chromatographic separation of the reaction products. Vapor diffusion of diethyl ether into the concentrated fourth eluent gave deep red crystals. A preliminary X-ray structural analysis disclosed that this compound is a dinuclear complex having linear Os−O−Os moiety with two monodentate acetate in both trans positions to the oxide bridge. IR (KBr)/cm^{-1}: ν(CO) 1685 s, 1620 m, 1493 m, 1460 s, 1372 m, 1260 s, 1244 s, 1222 s, 1074 m, 1022 m, 978 w, 928 w, 784 m, 763 m, 700 m, 692 m, 650 m, 557 w, 504 w, ν(Os−Cl) 328 m. ^{1}H NMR (CD_3CN)/ppm: δ 1.64 (s, 6H), 7.30 (t, 8H), 7.69 (tt, 4H), 8.72 (dd, 8H). Anal. Calcd for $C_{24}H_{26}Cl_4N_4O_5Os_2$: C, 29.64; H, 2.69; N, 5.76. Found: C, 29.42; H, 2.73; N, 6.04.

Other fractions did not give well identified products.

Pyridine-Exchange Reactions. A 100-fold excess of pyridine-d_5 was added to the solution of **1** in $(CD_3)_2SO$ (10 mg/1 mL) at 20 °C. The sample solution was quickly placed in the NMR cell compartment which was kept at 20 °C. The exchange reaction was followed at a certain interval until signals from coordinated pyridine completely disappeared.

X-ray Structural Determinations. X-ray data of **1**, **2**, and (Et_4N)[**3**] were collected with graphite-monochromated Mo Kα radiation on a Rigaku AFC-5R diffractometer at 20 °C. Each unit cell parameter was obtained by least-squares refinement of 25 reflections ($25 \leq 2\theta \leq 30°$). The intensities of three standard reflections for each compound, monitored every 150 reflections, showed no appreciable decay during the data collection. Absorption correction was made for all the three compounds.

The crystal structures were solved by standard heavy-atom procedures. The positional and thermal parameters were refined by the block-diagonal-matrix least-squares method. The minimized function was $\sum w(|F_o| - |F_c|)^2$, where $w^{-1} = \sigma^2(|F_o|) + (0.015\ |F_o|)^2$. No attempt was made to locate hydrogen atoms in the structure analysis. In the final cycle of the refinement, parameter shifts were less than 0.1σ. No correction was made for secondary extinction. The atomic scattering factors for neutral atoms, with correction for anomalous dispersion of Os^0 and Cl^0, were used throughout the analysis.[21] Computational work was carried out by using standard programs in UNICS III[22] and ORTEP.[23] Further crystallographic data are given in Table 1. Listings of the non-hydrogen atom coordinates are given in Tables 2−4, and selected bond distances and angles are summarized in Table 5. Anisotropic thermal parameters (Table S1−S3) and full listings of bond distances and angles (Table S4−S6) are provided as supplementary materials.

X-ray Photoelectron Spectroscopy. Ground samples were pressed between two pieces of indium foil. The pieces were then separated and one of them stuck to a Ni metal plate mounted for analysis. Spectra were obtained by a VG ESCALAB 200X instrument using Mg Kα exciting radiation at ambient temperature and pressures less than 10^{-8} Torr. Binding energies were determined by computer fitting of the measured spectra. Sample charging was corrected by reference to the C 1s peak at 285.0 eV.

Electrochemical Measurements. Cyclic voltammetry was performed with a Hokuto HA-501G potentiostat and a Hokuto HB-105 function generator equipped with a Graphtec WX2400 X-Y recorder. The working and the counter electrodes were a glassy-carbon disk and a platinum wire, respectively. Cyclic voltammograms were recorded at a scan rate of 50 mV/s. The sample solutions (ca. 1.0 mM) in 0.1 M TBAP−acetonitrile were deoxygenated with a stream of argon. The reference electrode was Ag/AgCl and the half-wave potential of Fc^+/Fc ($E_{1/2}(Fc^{+/0})$ vs Ag/AgCl) was +0.440 V.

Controlled-potential coulometry was carried out in 0.1 M TBAP−acetonitrile with a standard H-type cell with a Hokuto HA-501G potentiostat and a Hokuto HF-201 coulometer. The working electrode was made of platinum gauze, and the working compartment was separated from the counter compartment by a sintered-glass disk.

Other Measurements. The ^{1}H NMR spectra were obtained at 270 MHz with a JEOL JNM-EX270 spectrometer. ^{1}H chemical shifts were measured relative to the methyl resonance of TMS. UV−visible spectra were recorded on a Jasco Ubest-30 spectrophotometer at 20 °C. IR spectra were recorded on a Hitachi 270−50 infrared spectrophotometer.

(20) Salmon, D. J.; Walton, R. A. *Inorg. Chem.* **1978**, *17*, 2379−2382.

(21) *International Tables for X-ray Crystallography*; Ibers, J. A. Hamilton, W. C.; Kynoch: Birmingham, England, 1974; Vol. IV.

(22) Sakurai, T.; Kobayashi, K. *Rikagaku Kenkyuusho Hokoku (Rep. Inst. Phys. Chem. Res.)* **1979**, *55*, 69.

(23) Johnson, C. K. *ORTEP II*. Report ORNL-5138; Oak Ridge National Laboratory: Oak Ridge, TN, 1976.

Table 1. Crystallographic Data for X-ray Diffraction Studies

	$[OsO_2Cl_2(py)_2]$	$[Os^{IV}_2(\mu\text{-}O)Cl_5(CH_3CO_2)(py)_4]$	$(Et_4N)[Os^{III}Os^{IV}(\mu\text{-}O)Cl_5(CH_3CO_2)(py)_4]$
formula	$C_{10}H_{10}Cl_2N_2O_2Os$	$C_{22}H_{23}Cl_5N_4O_3Os_2$	$C_{30}H_{43}Cl_5N_5O_3Os_2$
cryst syst	tetragonal	monoclinic	orthorhombic
space group	$P4_12_12$	$P2_1/c$	$Pcab$
a /Å	10.452(1)	18.007(2)	20.895(4)
b /Å	10.452(1)	10.378(2)	25.120(5)
c /Å	12.149(1)	15.529(2)	14.149(9)
β /deg	90	104.53(1)	90
V /Å^3	1327.3(2)	2809.1(6)	7426(4)
Z	4	4	8
d_{calcd} /(g/cm^3)	2.26	2.25	1.93
cryst size /mm	0.09 × 0.05 × 0.34	0.10 × 0.21 × 0.45	0.26 × 0.07 × 0.25
scan range /deg	1.0 + 0.4 tan θ	1.5 + 0.4 tan θ	0.78 + 0.3 tan θ
scan mode	ω–2θ	ω–2θ	ω–2θ
scan speed /(deg min^{-1})	6	6	6
$2\theta_{max}$ /deg	60	60	50
μ(Mo Kα) /cm^{-1}	100.2	95.6	72.5
no. of unique reflns	1187	8909	7193
no. of obsd reflns	879, $F_o > 6\sigma(F_o)$	6019, $F_o > 3\sigma(F_o)$	3813, $F_o > 6\sigma(F_o)$
R[a]	0.028	0.057	0.047
R_w[a]	0.030	0.061	0.054

[a] $R = \Sigma||F_o| - |F_c||/\Sigma|F_o|$; $R_w = [\Sigma w(|F_o| - |F_c|)^2/\Sigma w|F_o|^2]^{1/2}$.

Results and Discussion

Preparation of the Complexes. The complex **1** was first prepared by Griffith and co-workers.[19] Their procedure involves the reaction of $K_2[OsO_2(OH)_4]$ with pyridine in water followed by the addition of HCl. We prepared **1** by adding pyridine to the reaction mixture of OsO_4 and HCl in EtOH. We thought that these two procedures may give different geometrical isomers with respect to Cl^- and py ligands. Thus we also prepared $[OsO_2Cl_2(py)_2]$ by the Griffith et al. method. However, the ^{1}H NMR and IR data of both the samples were identical with each other and with those reported by Griffith and co-workers.[19] Furthermore, we found that the compounds obtained from these two different procedures crystallize in the same space group and have the identical structure with two pyridine ligands in a *cis* configuration (vide infra). The ^{1}H NMR spectra of **1** did not show any temperature dependence even at 60 °C. There is no sign of the existence of isomeric forms in the solution. We concluded that the geometric structure as found by X-ray analysis is retained in solution.

The reactions between **1** and refluxing CH_3COOH–$(CH_3CO)_2O$ mixtures provided a mixture of several species, from which $[Os^{IV}_2(\mu\text{-}O)Cl_5(CH_3CO_2)(py)_4]$ (**2**) was separated out as a major product by column chromatography. The pyridine ligands coordinated to each osmium atom in **2** are in a *trans* configuration. The other structurally characterized species, $[Os^{IV}_2(\mu\text{-}O)Cl_4(CH_3CO_2)_2(py)_4]$ (**4**), also take a *trans* configuration at each osmium ion with respect to two pyridine ligands. It is not possible to conclude at this stage that the *trans* configuration of pyridine ligands would be preferred in the Os–O–Os complexes, because of low yield of these products and the failure to characterize other reaction products. The ^{1}H NMR spectrum of **2** in CD_3CN shows two sets of signals of pyridine. The complex **4** shows that all pyridine ligands are equivalent. The spectra of these complexes do not show any sign of the existence of isomeric forms in solution. Thus the solid state structure is retained in the solution. The reduction of **2** to $[\mathbf{3}]^-$ in acetonitrile either electrochemically or chemically with hydrazine monohydrate proceed quantitatively by judging from the visible absorption pattern and peak intensities. The mixed-valence compound $[\mathbf{3}]^-$ was isolated as a Et_4N^+ salt after the chemical reduction in acetonitrile. The *trans* configuration of **2** is retained during the reduction.

The *cis*–*trans* isomerization with respect to pyridine ligands occurred during the reaction between **1** and refluxing CH_3COOH–$(CH_3CO)_2O$ mixtures as far as the identified products are concerned. On addition of pyridine-d_5 to the $(CD_3)_2SO$ solution of **1**, signal intensities of the coordinated pyridine decrease with simultaneous increase in those of the free pyridine. The signal intensities of the coordinated pyridine have completely disappeared within 3 h at 20 °C. The change should be due to the substitution of pyridine-d_5 for the coordinated pyridine.

$$[OsO_2Cl_2(py)_2] + 2py\text{-}d_5 \rightarrow [OsO_2Cl_2(py\text{-}d_5)_2] + 2py$$

Thus the complex **1** is labile within the time scale of its conversion to the dinuclear Os–O–Os complexes.

Table 2. Fractional Coordinates and Isotropic Thermal Parameters (Å^2) for $[OsO_2Cl_2(py)_2]$

atom	x	y	z	B_{eq}
Os	0.0845(1)	0.0845(1)	0.0	2.62(1)
Cl	0.0874(3)	0.3041(2)	0.0420(2)	4.0(1)
O	0.0370(6)	0.1126(6)	−0.1339(5)	3.4(2)
N(11)	−0.1147(6)	0.0767(7)	0.0411(6)	3.1(2)
C(12)	−0.2002(8)	0.1450(9)	−0.0160(8)	3.3(2)
C(13)	−0.3295(9)	0.138(1)	0.0073(9)	4.3(3)
C(14)	−0.3723(9)	0.064(1)	0.0945(8)	4.6(3)
C(15)	−0.283(1)	−0.009(1)	0.1540(9)	5.0(3)
C(16)	−0.154(1)	0.001(1)	0.1269(7)	3.9(3)

Structure. The molecular structure of **1** is shown in Figure 1. The osmium atom lies on a crystallographically imposed 2-fold axis. Selected bond lengths and angles are given in Table 5. The geometry of the molecule is a distorted octahedron with the pyridine ligands or chloro ligands in a *cis* configuration and with an O–Os–O′ angle of 170.4(3)°. The bent *trans*-osmyl moiety is common to *trans*-dioxo osmium(VI) complexes; $[OsO_2(OH)_2(phen)]$ (166.2(2)°),[24] $[OsO_2(3\text{-}t\text{-}Bu\text{-}saltmen)]$ (176.6(4)°),[25] and $[OsO_2(o\text{-}oxobenzoato)(py)_2]$ (169.8(3)°).[26] The Os–O distance of 1.725(6) Å is also comparable to those in these osmium(VI) compounds.

The X-ray structure analysis disclosed that **2** is a dinuclear complex having a linear Os–O–Os unit in which the Os···Os

(24) Galas, A. M. R.; Hursthouse, M. B.; Behrman, E. J.; Midden, W. R.; Green, G.; Griffith, W. P. *Transition Met. Chem. (Weinheim, Ger.)* **1981**, *6*, 194–195.
(25) Che, C.-M.; Cheng, W.-K.; Mak, T. C. W. *Inorg. Chem.* **1988**, *27*, 250–253.
(26) Hinckley, C. C.; Kibala, P. A.; Robinson, P. D. *Acta Crystallogr.* **1987**, *C43*, 842–844.

Table 3. Fractional Coordinates and Isotropic Thermal Parameters (Å^2) for $[Os^{IV}_2(\mu\text{-}O)Cl_5(CH_3CO_2)(py)_4]$

atom	x	y	z	B_{eq}
Os(1)	0.18448(3)	0.15468(4)	0.23531(3)	2.32(1)
Os(2)	0.34219(3)	−0.06880(4)	0.25730(3)	2.30(1)
Cl(11)	0.1704(2)	0.1105(3)	0.3793(2)	3.4(1)
Cl(12)	0.1849(2)	0.2117(3)	0.0878(2)	3.8(1)
Cl(21)	0.3009(2)	−0.1907(3)	0.3650(2)	3.4(1)
Cl(22)	0.4434(2)	−0.2124(3)	0.2743(2)	3.6(1)
Cl(23)	0.3924(2)	0.0402(3)	0.1504(2)	3.7(1)
O(1)	0.2638(4)	0.0416(6)	0.2452(4)	2.3(2)
N(11)	0.2637(5)	0.2991(8)	0.2857(6)	2.8(2)
C(12)	0.2578(8)	0.373(1)	0.3561(8)	3.6(4)
C(13)	0.3131(9)	0.463(1)	0.3953(9)	4.8(4)
C(14)	0.3794(9)	0.475(1)	0.361(1)	5.0(5)
C(15)	0.3867(8)	0.399(1)	0.290(1)	4.3(4)
C(16)	0.3241(8)	0.313(1)	0.2524(9)	4.0(4)
N(21)	0.1035(5)	0.0099(9)	0.1870(6)	3.1(3)
C(22)	0.0359(8)	0.034(1)	0.1282(9)	3.9(4)
C(23)	−0.0174(9)	−0.063(1)	0.099(1)	5.2(5)
C(24)	−0.0020(8)	−0.189(1)	0.1268(9)	4.6(4)
C(25)	0.0657(9)	−0.214(1)	0.1876(9)	4.7(4)
C(26)	0.1193(7)	−0.114(1)	0.2191(8)	3.2(3)
N(31)	0.2768(5)	−0.1851(8)	0.1558(6)	3.0(3)
C(32)	0.2735(7)	−0.315(1)	0.1663(9)	3.7(4)
C(33)	0.2301(9)	−0.392(1)	0.0962(9)	4.6(4)
C(34)	0.1903(9)	−0.336(1)	0.019(1)	4.9(4)
C(35)	0.1920(8)	−0.202(1)	0.0091(9)	4.4(4)
C(36)	0.2363(7)	−0.128(1)	0.0787(8)	3.5(3)
N(41)	0.4100(6)	0.0472(8)	0.3597(6)	2.8(2)
C(42)	0.3748(9)	0.089(1)	0.4250(8)	4.1(4)
C(43)	0.4195(9)	0.171(1)	0.4919(8)	4.3(4)
C(44)	0.4919(9)	0.205(1)	0.4936(9)	4.8(4)
C(45)	0.5246(9)	0.159(1)	0.4271(9)	5.2(5)
C(46)	0.4806(7)	0.082(1)	0.3602(8)	3.4(3)
O(A1)	0.0991(5)	0.2741(7)	0.2228(5)	3.6(2)
O(A2)	0.1266(7)	0.481(1)	0.2262(9)	8.3(5)
C(A1)	0.0867(8)	0.395(1)	0.1941(9)	4.1(4)
C(A2)	0.013(1)	0.413(2)	0.122(1)	7.1(6)

Table 4. Fractional Coordinates and Isotropic Thermal Parameters (Å^2) for $(Et_4N)[Os^{III}Os^{IV}(\mu\text{-}O)Cl_5(CH_3CO_2)(py)_4]$

atom	x	y	z	B_{eq}
Os(1)	0.07595(3)	0.08773(3)	0.20926(4)	2.49(1)
Os(2)	0.12470(3)	0.22909(3)	0.19058(4)	2.43(1)
Cl(11)	0.1734(2)	0.0651(2)	0.2868(3)	3.8(1)
Cl(12)	−0.0240(2)	0.1006(2)	0.1313(3)	3.7(1)
Cl(21)	0.2349(2)	0.2040(2)	0.1919(3)	3.9(1)
Cl(22)	0.1573(2)	0.3197(2)	0.1745(3)	4.7(1)
Cl(23)	0.0170(2)	0.2600(2)	0.1887(3)	3.5(1)
O(1)	0.1003(4)	0.1582(4)	0.2001(7)	2.4(2)
O(A1)	0.0569(5)	0.0073(4)	0.2125(8)	3.7(3)
O(A2)	−0.0328(6)	−0.0019(5)	0.2971(9)	6.1(4)
C(A1)	0.0108(8)	−0.0198(7)	0.246(1)	4.1(5)
C(A2)	0.013(1)	−0.0775(7)	0.222(1)	5.6(7)
N(11)	0.0342(6)	0.1055(5)	0.3403(8)	2.8(4)
C(12)	0.0012(7)	0.1508(6)	0.351(1)	2.9(4)
C(13)	−0.0223(8)	0.1645(7)	0.441(1)	3.8(5)
C(14)	−0.0123(8)	0.1335(7)	0.520(1)	4.4(6)
C(15)	0.0207(9)	0.0847(7)	0.506(1)	4.7(6)
C(16)	0.0449(8)	0.0707(7)	0.416(1)	4.1(5)
N(21)	0.1183(6)	0.0715(5)	0.0782(8)	3.3(4)
C(22)	0.1721(7)	0.0993(6)	0.051(1)	3.2(5)
C(23)	0.1976(8)	0.0916(7)	−0.040(1)	4.1(5)
C(24)	0.1708(9)	0.0555(8)	−0.102(1)	5.1(6)
C(25)	0.1166(8)	0.0262(7)	−0.072(1)	4.4(6)
C(26)	0.0907(8)	0.0370(7)	0.018(1)	3.8(5)
N(31)	0.1245(6)	0.2211(5)	0.0431(8)	3.3(4)
C(32)	0.1746(8)	0.2401(7)	−0.009(1)	3.9(5)
C(33)	0.1733(9)	0.2334(9)	−0.109(1)	5.2(6)
C(34)	0.121(1)	0.2059(9)	−0.151(1)	6.7(8)
C(35)	0.0704(9)	0.1869(7)	−0.097(1)	4.7(6)
C(36)	0.0733(8)	0.1949(7)	0.002(1)	3.7(5)
N(41)	0.1260(5)	0.2362(5)	0.3395(8)	2.7(3)
C(42)	0.1017(8)	0.2819(7)	0.381(1)	3.7(5)
C(43)	0.1006(8)	0.2872(7)	0.479(1)	4.1(5)
C(44)	0.1274(9)	0.2448(8)	0.534(1)	5.1(6)
C(45)	0.1531(8)	0.1974(9)	0.491(1)	5.3(7)
C(46)	0.1522(7)	0.1929(7)	0.391(1)	3.9(5)
N(1)	0.2045(6)	−0.0589(7)	0.614(1)	5.3(5)
C(1)	0.174(2)	−0.072(1)	0.712(3)	17(2)
C(2)	0.156(1)	−0.067(1)	0.537(2)	11(1)
C(3)	0.231(1)	−0.002(1)	0.618(2)	11(1)
C(4)	0.259(1)	−0.093(1)	0.588(2)	14(1)
C(5)	0.180(2)	−0.120(1)	0.740(3)	18(2)
C(6)	0.167(2)	−0.049(1)	0.441(1)	13(1)
C(7)	0.174(1)	0.0413(9)	0.624(2)	7.1(8)
C(8)	0.319(2)	−0.083(1)	0.625(3)	16(2)

distance and the Os(1)−O(1)−Os(2) angle are 3.616(1) Å and 178.8(4)°, respectively (Figure 2). The coordination environment of each osmium atom is nonequivalent; a monodentate acetate ion coordinates to Os(1) in a *trans* position to bridging oxo ligand whereas a chloride ion coordinates to Os(2). The equatorial ligands of the two osmium ions are not different from each other. The compound **2** is the first (μ-oxo)diosmium(IV) complex with an unsymmetric ligand environment. As seen in Table 5, the four equatorial *cis*-to-oxo Os−Cl and Os−N bond lengths are almost identical with each other in **2**. This suggests that there is only a slight charge difference between the two osmium atoms. The Os(1)−O(1) distance (1.826(7) Å) is longer than the Os(2)−O(1) distance (1.790(7) Å). The structural characteristics of **2** are compared with other μ-oxo diosmium(IV) complexes (Table 6). The average Os−O_b distance of 1.808 Å in **2** is slightly longer than that of $Cs_4[Os_2OCl_{10}]$ (1.778(2) Å)[27] and that of $Os_2O(dppm)_2Cl_6$ (1.792(1) Å).[28,29] The axial Os(2)-Cl(22) bond (2.318(3) Å) is ca. 0.04−0.05 Å shorter than the equatorial Os−Cl bonds. This feature is also seen in the Os−Cl distance in axial (2.307(3) Å) and equatorial positions (2.360(3), 2.387(3) Å) of $Os_2O(dppm)_2Cl_6$,[28] while $Cs_4[Os_2OCl_{10}]$[27] displays an opposite tendency. The average Os−N(py) distance of 2.099 Å is ca. 0.04 Å less than that of **1** in spite of the higher oxidation state of osmium in **1**. This is because of the trans influence of a chloride ion to the Os−N(py) distance in **1**. The C(A1)−O(A1) and C(A1)−O(A2) distances in the acetate ion are 1.33(1) and 1.18(2) Å, in which the former and the latter may correspond to the single bond and the double bond, respectively. The coordination plane defined by Cl(11), Cl(12), N(11), and N(21) and that defined by Cl(21), Cl(23), N(31), and N(41) are twisted along the Os···Os axis by 25.8° probably due to a steric hindrance between pyridine rings. The dihedral angles between py(1) and py(2), between py(3) and py(4), between py(1) and py(4), and between py(2) and py(3) are 81.9(5), 86.3(11), 9.2(5), and 27.5(10)°, respectively.

The X-ray structure analysis disclosed that $[\mathbf{3}]^-$ is crystallized with Et_4N^+ in a 1:1 ratio; thus, the average oxidation state of osmium ions in the complex anion is +3.5. This is the first structural analysis of a mixed-valence $Os^{III}Os^{IV}$ complex with the linear Os−O−Os moiety. The observation of the nearly identical $Os-Cl_{equatorial}$ and Os−N distances between two Os ions indicates that the oxidation state of two Os ions is not significantly different from each other. The overall structure of the complex anion (Figure 3) is very similar to that of **2**. Important bond lengths of **2** and $[\mathbf{3}]^-$ are compared in Figure 4. The Os(1)−O(1) (1.847(9) Å) and Os(2)−O(1) distances

(27) Tebbe, K.-F.; von Schnering, H. G. *Z. Anorg. Allg. Chem.* **1973**, *396*, 66−80.

(28) Chakravarty, A. R.; Cotton, F. A.; Schwotzer, W. *Inorg. Chem.* **1984**, *23*, 99−103.

(29) It may not be appropriate to refer to the Os···Os distance of $Os_2O(dppm)_2Cl_6$ because the bridging ligand dppm would affect the Os···Os and thus the Os−O_b distances.

Table 5. Selected Bond Lengths and Angles for $[OsO_2Cl_2(py)_2]$ (**1**), $[Os^{IV}_2(\mu\text{-}O)Cl_5(CH_3CO_2)(py)_4]$ (**2**), $(Et_4N)[Os^{III}Os^{IV}(\mu\text{-}O)Cl_5(CH_3CO_2)(py)_4]$ ((Et_4N)[**3**])

	1	**2**	$[\mathbf{3}]^-$
	Bond Lengths (Å)		
Os(1)···Os(2)		3.616(1)	3.704(1)
Os–Cl	2.351(2)		
Os(1)–Cl(11)		2.357(3)	2.383(4)
Os(1)–Cl(12)		2.368(3)	2.384(4)
Os(2)–Cl(21)		2.362(3)	2.387(4)
Os(2)–Cl(22)		2.318(3)	2.386(5)
Os(2)–Cl(23)		2.367(3)	2.381(4)
Os–O	1.725(6)		
Os(1)–O(1)		1.826(7)	1.847(9)
Os(2)–O(1)		1.790(7)	1.857(9)
Os(1)–O(A1)		1.946(8)	2.059(10)
Os–N(11)	2.143(7)		
Os(1)–N(11)		2.082(8)	2.097(11)
Os(1)–N(21)		2.097(9)	2.095(12)
Os(2)–N(31)		2.096(9)	2.097(11)
Os(2)–N(41)		2.120(8)	2.114(11)
O(A1)–C(A1)		1.33(1)	1.28(2)
O(A2)–C(A1)		1.18(2)	1.24(2)
C(A1)–C(A2)		1.52(2)	1.49(3)
	Bond Angles (deg)		
Cl–Os–Cl′	91.3(1)		
Cl–Os–O	92.4(2)		
Cl–Os–O′	94.3(2)		
Cl–Os–N(11)	89.9(2)		
Cl–Os–N(11′)	178.3(2)		
O–Os–O′	170.4(3)		
O–Os–N(11)	86.9(3)		
O–Os–N(11′)	86.2(3)		
N(11)–Os–N(11′)	88.9(3)		
Os(1)–O(1)–Os(2)		178.8(4)	179.9(6)
Cl(11)–Os(1)–Cl(12)		173.4(1)	173.9(2)
Cl(11)–Os(1)–O(1)		93.6(2)	91.5(3)
Cl(11)–Os(1)–O(A1)		87.0(3)	85.4(3)
Cl(11)–Os(1)–N(11)		90.6(3)	90.0(3)
Cl(11)–Os(1)–N(21)		88.2(3)	90.0(4)
Cl(12)–Os(1)–O(1)		92.8(2)	94.5(3)
Cl(12)–Os(1)–O(A1)		86.5(3)	88.5(3)
Cl(12)–Os(1)–N(11)		90.9(3)	90.9(3)
Cl(12)–Os(1)–N(21)		90.2(3)	89.3(4)
O(1)–Os(1)–O(A1)		179.1(3)	174.4(4)
O(1)–Os(1)–N(11)		89.0(3)	88.4(4)
O(1)–Os(1)–N(21)		91.6(3)	90.5(5)
O(A1)–Os(1)–N(11)		91.6(3)	96.2(5)
O(A1)–Os(1)–N(21)		87.7(3)	84.9(5)
N(11)–Os(1)–N(21)		178.7(4)	178.9(5)
Cl(21)–Os(2)–Cl(22)		87.3(1)	88.7(2)
Cl(21)–Os(2)–Cl(23)		175.0(1)	176.3(2)
Cl(21)–Os(2)–O(1)		92.1(2)	90.7(3)
Cl(21)–Os(2)–N(31)		90.4(3)	89.1(4)
Cl(21)–Os(2)–N(41)		89.9(3)	90.1(3)
Cl(22)–Os(2)–Cl(23)		87.7(1)	87.6(2)
Cl(22)–Os(2)–O(1)		179.4(2)	178.6(3)
Cl(22)–Os(2)–N(31)		89.6(3)	89.8(4)
Cl(22)–Os(2)–N(41)		89.5(3)	90.6(4)
Cl(23)–Os(2)–O(1)		92.9(2)	93.0(3)
Cl(23)–Os(2)–N(31)		89.4(3)	91.0(4)
Cl(23)–Os(2)–N(41)		90.3(3)	89.7(3)
O(1)–Os(2)–N(31)		90.6(3)	88.9(5)
O(1)–Os(2)–N(41)		90.3(3)	90.7(4)
N(31)–Os(2)–N(41)		179.1(4)	179.1(5)
Os(1)–O(A1)–C(A1)		134.1(9)	133(1)
O(A1)–C(A1)–O(A2)		123(1)	125(2)
O(A1)–C(A1)–C(A2)		114(1)	114(2)
O(A2)–C(A1)–C(A2)		123(1)	120(2)
	Torsion Angles (deg)		
Cl(12)–Os(1)–Os(2)–Cl(23)		26.0(1)	27.7(1)
Cl(11)–Os(1)–Os(2)–Cl(21)		24.8(1)	26.9(1)
N(11)–Os(1)–Os(2)–N(41)		26.9(4)	26.7(4)
N(21)–Os(1)–Os(2)–N(31)		25.5(4)	26.0(5)

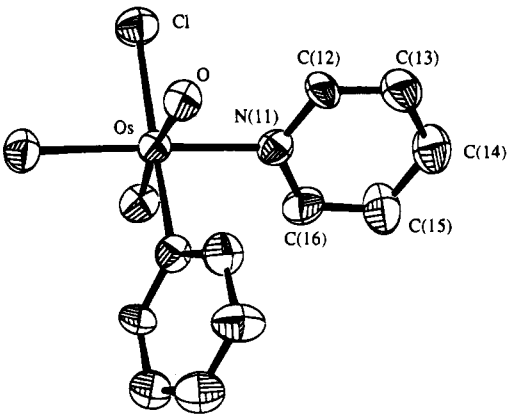

Figure 1. ORTEP drawing of $[OsO_2Cl_2(py)_2]$ with the atomic numbering scheme showing 50% probability thermal ellipsoids.

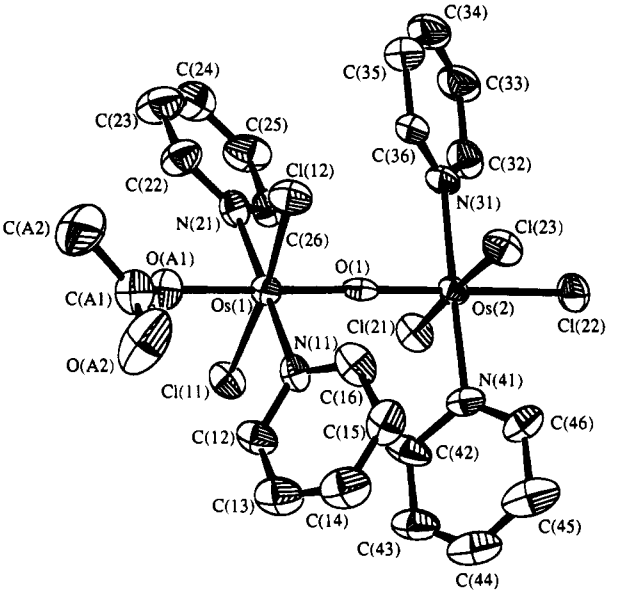

Figure 2. Molecular structure and atom labeling of $[Os^{IV}_2(\mu\text{-}O)Cl_5(CH_3CO_2)(py)_4]$. Thermal ellipsoids are drawn to illustrate 50% probability surfaces.

(1.857(9) Å), respectively, are 0.02 and 0.07 Å longer than those of **2**, with the smaller difference between the Os(1)–O(1) and Os(2)–O(1) distances in $[\mathbf{3}]^-$. The axial Os(2)–Cl(22) distance (2.386(5) Å) is elongated by ca. 0.06 Å from that of **2** and is now similar to the average equatorial Os–Cl distance (2.384 Å) which is ca. 0.02 Å longer than that of **2**. The average Os–N(py) distance (2.101 Å) is, however, practically unchanged by the reduction. The distance between the osmium atom and acetate oxygen atom (Os(1)–O(A1), 2.059(10) Å) is elongated by ca. 0.11 Å from that of **2**. It is apparent that the difference between the axial bond lengths in **2** and $[\mathbf{3}]^-$ is larger than that between the equatorial ones in **2** and $[\mathbf{3}]^-$; namely, the elongation of bond lengths occurred almost exclusively in the axial direction by reduction. The C–O distances in the acetate ion are similar in $[\mathbf{3}]^-$ (C(A1)–O(A1), 1.28(2) Å; C(A1)–O(A2), 1.24(2) Å), indicating that more significant π electron delocalization on the O–C–O bond in $[\mathbf{3}]^-$ than in **2**. The fact that the dihedral angle between acetate ion and the coordination plane of Os(1) defined by O(A1), O(1), N(11), and N(21) in $[\mathbf{3}]^-$ (28.2(5)°) is less than that in **2** (35.4(18)°) is also consistent with π electron delocalization. These phenomena are understood by considering the increase of π donation of acetate ion to the osmium atom. The coordination plane defined by Cl(11), Cl(12), N(11), and N(21) and that defined by Cl(21), Cl(23), N(31), and N(41) are twisted along the Os···Os

Table 6. Comparison of Selected Bond Distances (Å) and Bond Angles (deg) in Dinuclear Os(IV) Compounds with Os−O−Os Structure

compd	Os−O_b	Os−$Cl_{equatorial}$	Os−Cl_{axial}	Os−O−Os	ref
$[Os_2(\mu\text{-}O)Cl_5(CH_3CO_2)(py)_4]$ (**2**)	1.826(7), 1.790(7)	2.357(3), 2.368(3), 2.362(3), 2.367(3)	2.318(3)	178.8(4)	this work
$Cs_4[Os_2(\mu\text{-}O)Cl_{10}]$	1.778(2)	2.375(6), 2.371(6), 2.370(6), 2.367(6)	2.433(7)	180	27
$[Os_2(\mu\text{-}O)(dppm)_2Cl_6]$	1.792(1)	2.387(3), 2.360(3)	2.307(3)	180	28

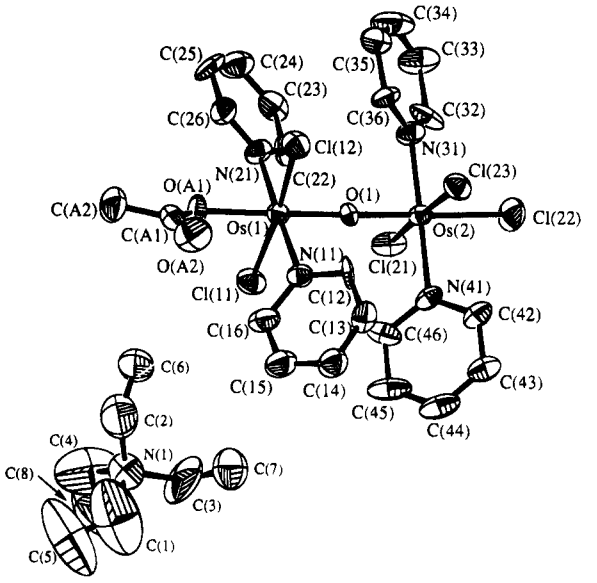

Figure 3. ORTEP diagram of $(Et_4N)[Os^{III}Os^{IV}(\mu\text{-}O)Cl_5(CH_3CO_2)(py)_4]$ with the atomic numbering scheme showing 50% probability thermal ellipsoids. The view direction is adjusted with that of $[Os^{IV}{}_2(\mu\text{-}O)Cl_5(CH_3CO_2)(py)_4]$.

axis by 26.8° in $[\mathbf{3}]^-$ which is similar to **2**. The dihedral angles between py(1) and py(2), between py(3) and py(4), between py(1) and py(4), and between py(2) and py(3) are 76.8(6), 87.0(6), 14.3(5), and 18.4(6)°, respectively, and again these values are similar to those in **2**.

Recently, a mixed-valence $Ru^{III}Ru^{IV}$ complex with a linear Ru−O−Ru moiety, $[\{(HCO_2)(NH_3)_4Ru\}_2(\mu\text{-}O)]Cl_3$, has been synthesized and structurally characterized.[30] The Ru−O_b (1.8240(6) Å) and Ru−$O_{formate}$ distances (2.033(3) Å) in the formate capped complex are ca. 0.03 Å shorter than the average Os−O_b (1.852 Å) and Os(1)−O(A1) distances (2.059(10) Å) in $[\mathbf{3}]^-$, respectively. A tendency for π electron delocalization on the O−C−O bond in the formate group is also seen in $[\{(HCO_2)(NH_3)_4Ru\}_2(\mu\text{-}O)]Cl_3$. The lack of structural information on the corresponding $Ru^{IV}{}_2$ complex prevents a detailed comparison among $Os^{III}Os^{IV}$, $Os^{IV}{}_2$, $Ru^{III}Ru^{IV}$, and $Ru^{IV}{}_2$ systems.

Redox Properties. $[Os_2(\mu\text{-}O)(CH_3COO)Cl_5(py)_4]$ (**2**) exhibits an irreversible oxidation wave with $E_{pa} = +1.68$ V, a reversible reduction process with $E_{1/2}{}^1 = +0.03$ V, and a quasi-reversible reduction process with $E_{1/2}{}^2 = -1.15$ V (Figure 5). The cathodic and anodic peak separation (ΔE_p) of both reduction processes are 60 mV, the i_{pa}/i_{pc} ratios are 1.0 ($E_{1/2}{}^1$) and 0.78 ($E_{1/2}{}^2$), and the $i_{pc}{}^1/i_{pc}{}^2$ ratio is 1.0. Controlled-potential coulometry for **2** at −0.4 V gave an electron stoichiometry of 0.95 ± 0.05 e/Os_2. Therefore both reduction processes are one electron processes and are represented by

$$[Os^{IV}{}_2(\mu\text{-}O)Cl_5(CH_3CO_2)(py)_4] + e^- \rightleftharpoons [Os^{III}Os^{IV}(\mu\text{-}O)Cl_5(CH_3CO_2)(py)_4]^-$$

$$[Os^{III}Os^{IV}(\mu\text{-}O)Cl_5(CH_3CO_2)(py)_4]^- + e^- \rightleftharpoons [Os^{III}{}_2(\mu\text{-}O)Cl_5(CH_3CO_2)(py)_4]^{2-}$$

As is seen in Figure 5, the mixed-valence state, $Os^{III}Os^{IV}$, is stable for a fairly wide range of potentials and the comproportionation constant, K_c, is calculated to be 8.87×10^{19} from the difference between half-wave potentials ($\Delta E_{1/2}$).[31] Bulk electrochemical reduction of a yellow-green solution of **2** at −0.4 V gave an orange solution whose absorption spectrum coincides quantitatively with that of the isolated $(Et_4N)[\mathbf{3}]$ in acetonitrile. The two-electron reduced species of **2** was found to be difficult to characterize at this stage because of its highly negative reduction potential.

The electrochemical behavior of **2** can be compared with that of $Os_2O(dppm)_2Cl_6$.[28] Two characteristic features are noted by comparison, although it is difficult to compare the absolute value of reduction potentials directly because of the different experimental condition (solvent and reference electrode). First of all, these compounds show one reversible reduction wave and one quasi-reversible or irreversible reduction wave with a large difference (more than 1 V) of the two reduction potentials. Thus

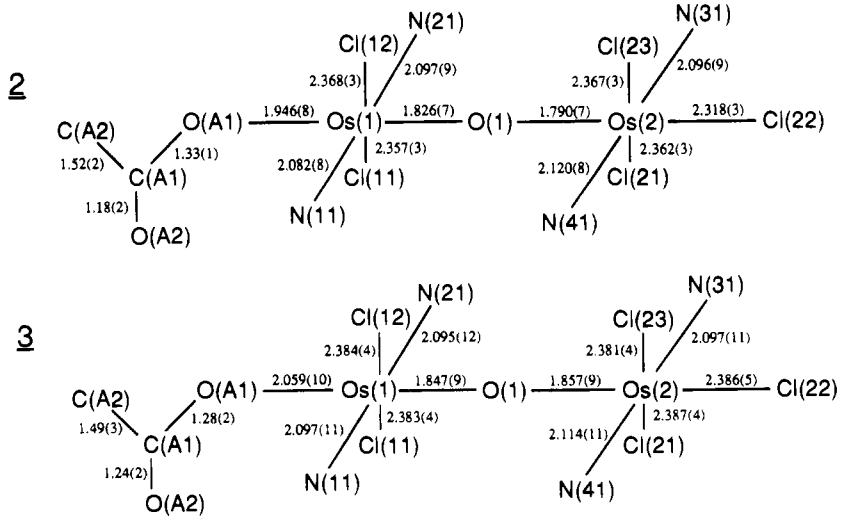

Figure 4. Comparison of important bond lengths between $[Os^{IV}{}_2(\mu\text{-}O)Cl_5(CH_3CO_2)(py)_4]$ (top) and $[Os^{III}Os^{IV}(\mu\text{-}O)Cl_5(CH_3CO_2)(py)_4]^-$ (bottom).

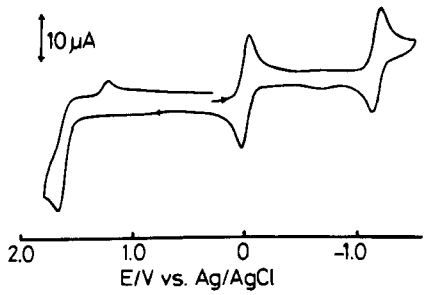

Figure 5. Cyclic voltammogram of $[Os^{IV}_2(\mu\text{-}O)Cl_5(CH_3CO_2)(py)_4]$ in 0.1 M TBAP–CH_3CN at a glassy-carbon electrode with a scan rate of 50 mV/s.

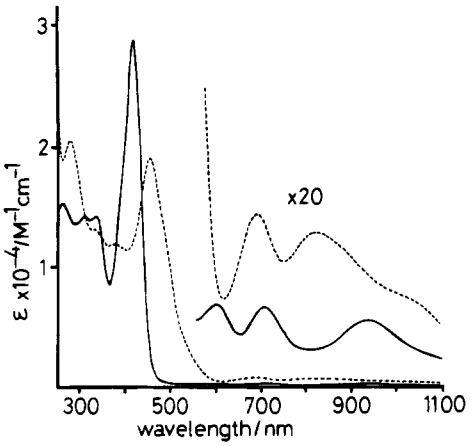

Figure 6. Absorption spectra of $[Os^{IV}_2(\mu\text{-}O)Cl_5(CH_3CO_2)(py)_4]$ (—) and $(Et_4N)[Os^{III}Os^{IV}(\mu\text{-}O)Cl_5(CH_3CO_2)(py)_4]$ (- -) in CH_3CN.

the $Os^{III}Os^{IV}$ mixed-valence state is fairly stable for these compounds and easy to obtain electrochemically ($E_{1/2}^1 \cong 0 \sim 0.3$ V). Second, the Os^{III}_2 state is unstable or difficult to characterize because of its highly negative reduction potential, although **2** seems to give the more stable Os^{III}_2 state. The electrochemical properties of $Os_2(\mu\text{-}O)(\mu\text{-}O_2CR)_2X_4(PR'_3)_2$ (X = Cl, Br; R = CH_3 or C_2H_5; PR'_3 = PPh_3, PEt_2Ph) have also been reported.[18] It is interesting that these compounds with bent Os–O–Os moiety show similar electrochemical behavior to **2**.

Electronic Structures. The UV–visible absorption spectra of **2** and (Et_4N)[**3**] are shown in Figure 6. In the spectrum of **2**, there are four intense bands at 261 (ϵ = 16 300 M^{-1} cm^{-1}), 306 (14 700), 335 (14 500), and 418 nm (29 000) and weaker ones at 598 (430), 704 (430), and 935 nm (350). The similar spectral features between **2** and $Os_2OCl_{10}^{4-}$ [32] indicate that the transitions may be attributed to their linear Os–O–Os unit. The most intense band at 418 nm may be ascribed to the π^{nb} to π^* transition by analogy with the assignment for $Os_2OCl_{10}^{4-}$.[32] It is impossible at this stage to propose further assignments.

In the spectrum of (Et_4N)[**3**], there are three intense bands at 278 (ϵ = 20 600 M^{-1} cm^{-1}), 380 (12 000), and 454 nm (19 200), two shoulders at around 330 (ca. 13 000) and 500 nm (ca. 7200), and weaker ones at 685 (720) and 819 nm (650). The most intense band appeared at longer wavelength (454 nm) in (Et_4N)[**3**] as compared with **2** (418 nm).

The mixed-valence compound (Et_4N)[**3**] has an odd electron. We measured X-ray photoelectron spectra of (Et_4N)[**3**] in order to clarify whether the odd electron is delocalized over the two osmium atoms or localized on one of the osmium atoms. The XPS was also measured for **1** and **2** for comparison (Table 7). The binding energy of 4f electrons, $Os(4f_{7/2})$, of **2** (53.2 eV) is in excellent agreement with those of $Os_2(\mu\text{-}O)(\mu\text{-}O_2CR)_2X_4(PPh_3)_2$ (X = Cl, Br; R = CH_3 or C_2H_5) (52.5–53.0 eV).[18] The binding energy of 4f electrons decreases with decrease of the formal oxidation state of the osmium atoms. No splitting of the peak was observed in the spectrum of $Os(4f_{7/2})$ region of (Et_4N)[**3**]. This observation suggests that the odd electron is delocalized over the two osmium atoms.

Table 7. XPS Data for Osmium Compounds

compd	formal oxidation state	Os(4f7/2) (eV)
$[OsO_2Cl_2(py)_2]$ (**1**)	+6	56.6
$[Os_2(\mu\text{-}O)(CH_3CO_2)Cl_5(py)_4]$ (**2**)	+4	53.2
$(Et_4N)[Os_2(\mu\text{-}O)(CH_3CO_2)Cl_5(py)_4]$ ((Et_4N)[**3**])	+3.5	51.4

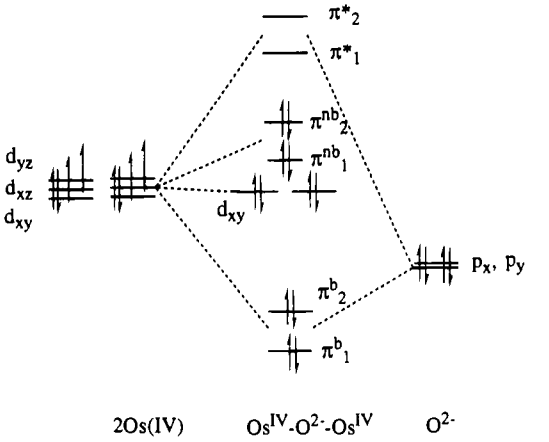

Figure 7. Qualitative molecular orbital description of bonding within the $Os^{IV}–O^{2-}–Os^{IV}$ moiety.

A qualitative molecular orbital scheme for the complexes **2** and $[\mathbf{3}]^-$ is given in Figure 7, which is obtained by modifying the model given by Dunitz and Orgel for the linear oxo–ruthenium complex, $[Ru_2OCl_{10}]^{4-}$.[33] Here, the difference in the apical ligand is neglected. The pair of π-bonding, nonbonding, and antibonding orbitals may split due to the coordination of two different ligands, Cl^- and pyridine, at equatorial sites by analogy with the MO diagram for the $[(AA)_2XRuORuX(AA)_2]^{n+}$ system (AA = 2,2′-bipyridine, 1,10-phenanthroline; X = Cl^-, NO_2^-, H_2O).[34] The exact order of d_{xy} and π^{nb} orbitals is uncertain at this stage. The short Os–O bond lengths of **2** are explained by the multiple-bond character with the π-bonding interaction in addition to the σ-one. The diamagnetism of **2** is consistent with the scheme as pointed out previously for $[Ru_2OCl_{10}]^{4-}$ [33] and $[Os_2OCl_{10}]^{4-}$.[32]

Structural comparison of **2** and $[\mathbf{3}]^-$ provides further information on the Os–O bond character of linear Os–O–Os complexes. The difference in the two Os–O bond lengths in **2** manifests the different contribution of the $d\pi$ orbitals of the two Os centers to the π orbitals. The longer Os(1)–O bond length indicates less contribution of the Os(1) $d\pi$ orbital to the occupied π bonding orbitals and more to the vacant antibonding orbitals. Occupation of π antibonding orbitals on reduction to $[\mathbf{3}]^-$ would weaken the π bonding character of the Os–O bonds and the difference in the bond lengths decreases. The bond lengths of Os and axial ligands also expand considerably as

(30) Emerson, J.; Clarke, M. J.; Ying, W.-L.; Sanadi, D. R. *J. Am. Chem. Soc.* **1993**, *115*, 11799–11805.
(31) Richardson, D. E.; Taube, H. *Inorg. Chem.* **1981**, *20*, 1278–1285.
(32) San Filippo, J., Jr.; Fagan, P. J.; Di Salvo, F. J. *Inorg. Chem.* **1977**, *16*, 1016–1021.
(33) Dunitz, J. D.; Orgel, L. E. *J. Chem. Soc.* **1953**, 2594–2596.
(34) Weaver, T. R.; Meyer, T. J.; Adeyemi, S. A.; Brown, G. M.; Eckberg, R. P.; Hatfield, W. E.; Johnson, E. C.; Murray, R. W.; Untereker, D. *J. Am. Chem. Soc.* **1975**, *97*, 3039–3048.

compared with the equatorial bond lengths. Thus, the π system would be extended to the axial ligands at least in **2**.

Acknowledgment. The authors are grateful to Prof. T. Kawamura at Gifu University and Prof. K. Tatsumi at Nagoya University for their valuable discussions. This work was supported by a Grant-in-Aid for Scientific Research (No. 05403008) and a Grant-in-Aid for Scientific Research on Priority Area of "Activation of Inactive Small Molecules" (05235202) from the Ministry of Education, Science and Culture of Japan and was partly supported by the Joint Studies Program (1993–1994) of the Institute for Molecular Science. A research grant from Suhara Memorial Foundation is also gratefully acknowledged.

Supplementary Material Available: Listings of anisotropic thermal parameters (Tables S1–S3) and bond lengths and angles (Tables S4–S6) (11 pages). Ordering information is given on any current masthead page.

IC940898R